

# Transport across interfaces in symmetric orbifolds

---

**Saba Asif Baig, Sanjit Shashi**

*Theory Group, Weinberg Institute, Department of Physics, University of Texas,  
2515 Speedway, Austin, Texas 78712, USA.*

*E-mail:* [sbaig@utexas.edu](mailto:sbaig@utexas.edu), [sshashi@utexas.edu](mailto:sshashi@utexas.edu)

**ABSTRACT:** A general classification of conformal interfaces has long been lacking in the literature. One approach is to map interfaces to conformal boundaries, then to use the tools of boundary CFT to extract specific physical data encoded by an associated boundary state. Guided by this, we examine how boundary states encode energy transport coefficients—i.e. transmission and reflection probabilities—of the related conformal interfaces in symmetric orbifold theories, which constitute a large class of irrational theories and are closely related to holographic setups. At the orbifold point, we find that the transport coefficients are only informed by untwisted-sector terms in the boundary states and so are averages of coefficients in the underlying seed theory. Following that, we then study the symmetric orbifold of the  $T^4$  sigma model ICFT dual to type IIB supergravity on the 3d Janus solution. The Janus solution can be used to compute transport coefficients of particular interfaces in the strongly coupled regime of the symmetric orbifold theory (far from the orbifold point). We compare these coefficients to that of the free theory, finding that the profile of the transmission coefficient changes functionally and overall increases with the coupling.

---

## Contents

<b>1</b>	<b>Introduction</b>	<b>2</b>
<b>2</b>	<b>Interface data in symmetric orbifold theories</b>	<b>4</b>
2.1	Twisted sectors of symmetric orbifolds	4
2.2	Building the boundary states	7
2.3	Transport coefficients from seed data	9
<b>3</b>	<b>The holographic symmetric orbifold of the <math>\mathbb{T}^4</math> ICFT</b>	<b>11</b>
3.1	3d Janus and holography	12
3.2	Strong-coupling transport from gravity waves	14
3.3	Weak-coupling transport from seed theory	17
3.4	Comparing across regimes	18
<b>4</b>	<b>Discussion</b>	<b>19</b>
4.1	Transport versus thermodynamics	20
4.2	The Janus boundary state	20
4.3	Other future directions	22

---

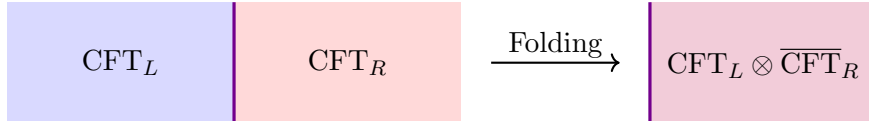


**Figure 1:** An ICFT consists of a “left” CFT and a “right” CFT glued together along a defect (left). This can be mapped to a BCFT (right) by folding along the defect.

## 1 Introduction

2-dimensional conformal field theories with boundaries have a long history in the literature [1, 2], with applications to both condensed matter theory [3, 4] and worldsheet string theory [5–8]. However, given some theory, the underlying classification principles of such boundaries consistent with conformal structure (particularly in irrational CFT) are unknown.

As a first pass to characterizing conformal boundaries, we can examine specific physical data that is “encoded” by the boundary. One example is the ground-state degeneracy  $g$  (also called the  $g$ -function) of the boundary state [9]. This is a  $c$ -number and is associated with a thermodynamic *boundary entropy*  $S_b = \log g$  [2]. Essentially,  $g$  counts the “boundary degrees of freedom.”

Instead of a CFT with a boundary, we may consider two CFTs glued along a defect surface (in 2d, a line) preserving (reduced) conformal symmetry. This defect is an interface between the constituent systems [10], so the full theory is called an *interface CFT (ICFT)*. Like with boundaries, a general classification of conformal interfaces is unknown. However, an ICFT can be mapped to a boundary (B)CFT by folding along the interface (Figure 1), so these are related problems (cf. [11]). In particular, physical parameters characterizing interfaces are encoded by boundary states, with the  $g$ -function being one example [12].

Nonetheless, interfaces make manifest additional physics encoded by the folded boundary states. One example is energy transport, which is characterized by *transport coefficients* associated with the interface [13, 14]. The proportion of energy transported across the interface is quantified by a transmission coefficient  $\mathcal{T}$ , while the proportion that is bounced back is described by a reflection coefficient  $\mathcal{R}$ . These transport coefficients are defined through expectation values of the stress tensor by [13] and sum to 1 (assuming unitarity).

The underlying motivation of this work is to advocate for transport coefficients as describing a facet of the physics of conformal defects apart from the  $g$ -function. This is a rather broad goal, so to narrow our focus we examine a particular class of CFT—*symmetric orbifold theories*. These are defined by taking  $N$  copies of some “seed” theory  $\mathcal{M}$  and quotienting by the permutations constituting the symmetric group  $S_N$ . Motivated by the recent classification of boundaries and  $g$ -functions in symmetric orbifolds [15],<sup>1</sup> our main reasons for considering these theories lie in both their tractability (given information about the seed theory) and their connections to holographic CFT (cf. [17, 18]). The general analysis of symmetric orbifold CFT at the orbifold point constitutes Section 2.

Furthermore, some symmetric orbifold theories may be understood directly at strong

<sup>1</sup>See also [16] for similar work in the context of string theory and holography.

coupling<sup>2</sup> via the AdS/CFT correspondence [20], thereby giving us access to a regime in which field-theoretic calculations typically become intractable. For example, type IIB supergravity on  $\text{AdS}_3 \times S^3 \times \mathbb{T}^4$  is dual to the symmetric orbifold of a  $\mathbb{T}^4$  sigma model at strong coupling and with a large number of copies, and this duality also persists in more stringy/weakly coupled regimes [21]. More pertinent to our purposes, we can describe a simple class of top-down conformal interfaces in this CFT and at strong coupling through a non-supersymmetric<sup>3</sup> dilatonic deformation of the  $\text{AdS}_3$  bulk. The resulting gravitational background is called Janus [24]. By using the holographic prescription proposed for “thin-brane” configurations [25] and further refined in subsequent work [26, 27], one may obtain transport coefficients encoded by particular boundary states in the strongly coupled sector of the ICFT dual to type IIB on Janus.

Indeed, the holographic transmission coefficients of the Janus interface have been obtained recently [27]. In Section 3, we will compare these coefficients against those of the Janus interface at the orbifold point, which we obtain via applying the procedure of Section 2 to an appropriate boundary state of the folded  $\mathbb{T}^4$  seed theory. The seed theory is four non-interacting copies of a free  $S^1$ -valued scalar field, each with a jump in mass along a defect. Under folding, each individual  $S^1$  theory maps to two non-interacting scalar fields on half space that together are taken to satisfy a “Neumann–Dirichlet” boundary condition [12]. Transport in the folded free scalar theory with this boundary condition has long been understood [13]. This procedure ultimately yields an approximate answer for transport coefficients in the weakly coupled regime of the  $\mathbb{T}^4$  symmetric orbifold theory.

Performing this type of strong-weak comparison is not a new application of the holographic nature of the Janus solution, although it has not been done for transport coefficients. [12] exploited the tractability of both the strongly coupled and weakly coupled regimes of the  $\mathbb{T}^4$  symmetric orbifold ICFT to study how the boundary entropies  $S_b$  of these interfaces run with coupling.<sup>4</sup> They found that  $S_b$  is highly insensitive to coupling, running only a small amount. Going further, a similar calculation in supersymmetric Janus [23] found an exact match between the strongly coupled and weakly coupled regimes. However, in our comparison, we find that  $\mathcal{T}$  changes much more nontrivially with coupling when the parameter characterizing the strength of the dilatonic deformation is not at the ends of its regime of validity.

This makes sense. Heuristically, quantities describing transport are more sensitive to coupling than those describing thermodynamics. The classic example is  $\mathcal{N} = 4$  supersymmetric Yang–Mills in which free energy [28, 29] only changes by a factor of  $\frac{3}{4}$  while shear viscosity of the SYM plasma [30–32] changes infinitely. Inspired by this story, we interpret our results as further evidence for the idea that transport is more sensitive to coupling than thermodynamics.

---

<sup>2</sup>We are referring to the marginal coupling which, when turned on, takes us away from the orbifold point [19]. This coupling makes the  $N$  copies of the theory interact.

<sup>3</sup>There are also supersymmetric deformations of the  $\text{AdS}_3 \times S^3 \times \mathbb{T}^4$  vacuum [22, 23].

<sup>4</sup>They assume the boundary entropy has no contributions from twist fields. In light of [15], a boundary state agreeing with this assumption is more consistent with a bulk geometrical interpretation (i.e. a supergravity state) but is also “atypical.” We discuss this more in the Section 4.2.

## 2 Interface data in symmetric orbifold theories

We start by schematically discussing the physical data of conformal interfaces in the symmetric orbifold of a *known* ICFT  $\mathcal{M}$ . In particular, the  $N$ -fold symmetric orbifold theory  $\mathcal{M}_N$  consists of  $N$  copies of  $\mathcal{M}$  modded out by the symmetric group  $S_N$  whose action is permutation of the factors:

$$\mathcal{M}_N = \mathcal{M}^{\otimes N} / S_N. \quad (2.1)$$

Here we focus on the “orbifold point” of the theory, in which the  $N$  copies are taken to be non-interacting. This can also be seen as the free sector of the theory.

Instead of dealing with conformal interfaces directly, it is practical to map them to conformal boundaries first via folding [13]. Suppose that the seed ICFT  $\mathcal{M}$  consists of two CFTs  $\mathcal{C}_L$  and  $\mathcal{C}_R$  glued along an interface. We map this to a seed BCFT  $\widetilde{\mathcal{M}} = \mathcal{C}_L \otimes \overline{\mathcal{C}}_R$ . This induces a mapping between  $\mathcal{M}_N$  and a symmetric orbifold  $\widetilde{\mathcal{M}}_N$  of the BCFT. Thus we can use the technology of boundary CFT, particularly that of boundary states, to study conformal interfaces (cf. [10, 11]).

Following [15], we start by assuming knowledge about interface (or boundary) data in the seed theory. Using this knowledge and the combinatorics of the symmetric group  $S_N$ , we may then establish a recipe for interface (or boundary) data in the associated symmetric orbifold theory at the orbifold point.

### 2.1 Twisted sectors of symmetric orbifolds

Let us first review the basic structure of symmetric orbifold theories, following [15]. There are two major differences between the spectra of the  $N$ -fold product theory  $\mathcal{M}^{\otimes N}$  and of the symmetric orbifold theory  $\mathcal{M}_N$ . The first is that only product states which are invariant under all permutations survive the orbifolding procedure, so the only states inherited from the  $N$ -fold product theory are those which are symmetric. These particular states constitute the so-called *untwisted sector* of  $\mathcal{M}_N$ .

The second difference is the presence of *twisted sectors* in the orbifolded theory. When we quotient by a permutation  $\sigma \in S_N$ , we are gluing together some of the copies of the seed theory in  $\mathcal{M}^{\otimes N}$ . The resulting states in the glued sector are “ $\sigma$ -twisted.”

In the full symmetric orbifold theory, we are modding out by all permutations in  $S_N$ , thereby forgetting the order of the copies. As a result, each twisted sector consists of totally symmetric sums of twisted states taken over all permutations of a particular cycle type. For example, in the  $N = 3$  case, we would sum together states twisted by permutations  $(12), (13), (23) \in S_3$  to get states in one of the twisted sectors, and we would similarly sum together states twisted by  $(123), (132) \in S_3$  to get those of the other twisted sector. See Figure 2 for a cartoon.

The permutations of a particular cycle type precisely constitute a particular conjugacy class of  $S_N$ . Furthermore, through this equivalence, the conjugacy classes each correspond to an integer partition of  $N$  (the cycle type). So, the number of twisted sectors in the symmetric orbifold theory matches the number of distinct integer partitions of  $N$ .

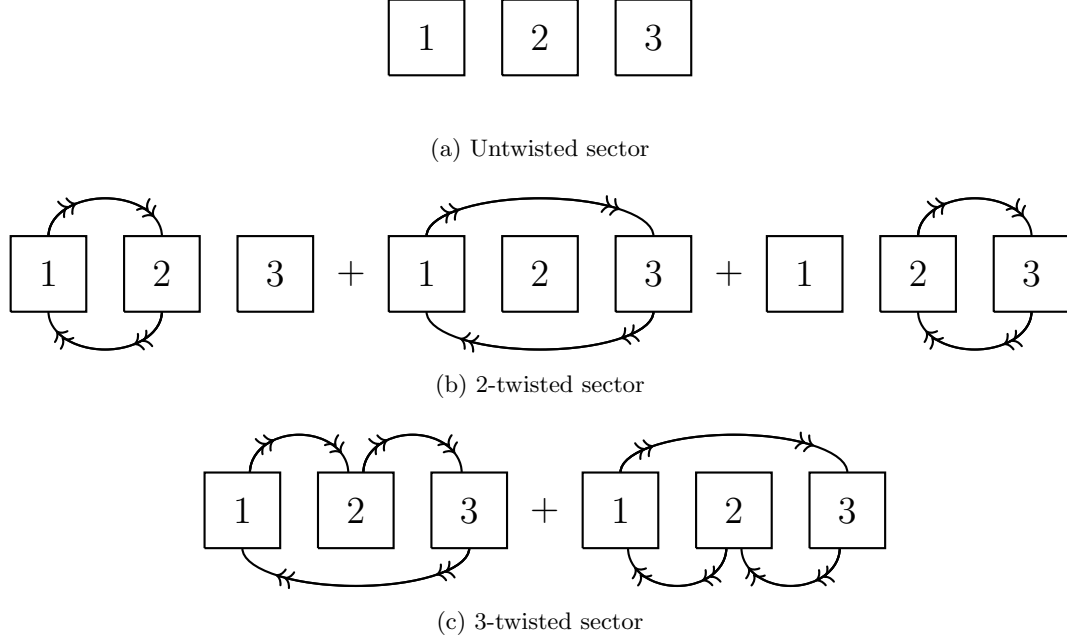


**Figure 2:** The different gluings corresponding to the various sectors of the symmetric orbifold theory  $\mathcal{M}_3 = \mathcal{M}^{\otimes 3}/S_3$ . The untwisted sector (a) consists purely of (symmetrized) product states. The 2-twisted sector (b) comes from gluing together any two copies of the seed theory  $\mathcal{M}$ . The 3-twisted sector arises from gluing together all three copies of  $\mathcal{M}$ .

**Twisted states** If we have a primary operator in the seed theory, then each twisted sector supports a twist of this operator. For example, consider a seed primary scalar of weight  $h$  and a single  $k$ -cycle  $\sigma = (a_1 a_2 \cdots a_k) \in S_N$  ( $k \leq N$ ). The  $\sigma$ -twisted state corresponding to this seed primary has weight

$$\sigma[h] = \frac{c}{24} \left( k - \frac{1}{k} \right) + \frac{h}{k}. \quad (2.2)$$

For a twisted sector corresponding to a more complicated cycle type with multiple disjoint cycles, we simply add the individual weights together. Specifically, consider a permutation  $\sigma = \sigma_1 \cdots \sigma_m$ , where each  $\sigma_i$  is a  $k_i$ -cycle and the different factors are disjoint. Then,

$$\sigma[h] = \sum_{i=1}^m \sigma_i[h]. \quad (2.3)$$

Observe that the weight of a twisted state only cares about the cycle type. As such, seed states twisted by different but conjugate elements of  $S_N$  will inherit the same weights. Thus the symmetrized sums of twisted seed primaries inherited by the symmetric orbifold theory are themselves primaries and may be labeled only by cycle type.

Each twisted sector has its own ground state realized as a twist of the seed vacuum state  $h = 0$ . The resulting primary operators in the symmetric orbifold theory are called *bare twists*. For example, consider again a single  $k$ -cycle  $\sigma$ . The bare twist by  $\sigma$  has weight

$$\sigma[0] = \frac{c}{24} \left( k - \frac{1}{k} \right), \quad (2.4)$$

and weights of bare twists by more complicated cycles can again be computed with (2.3).

As a quick example, we may compute the bare twists in the  $N = 4$  case. There are five conjugacy classes of  $S_4$  corresponding to the integer partitions of 4. The associated ground-state weights (taking particular representatives of the conjugacy classes) are

$$\begin{aligned}
1 + 1 + 1 + 1 &\mapsto \mathbb{1}[0] = 0, \\
1 + 1 + 2 &\mapsto (1\,2)[0] = \frac{c}{16}, \\
1 + 3 &\mapsto (1\,2\,3)[0] = \frac{c}{9}, \\
2 + 2 &\mapsto ((1\,2)(3\,4))[0] = \frac{c}{8}, \\
4 &\mapsto (1\,2\,3\,4)[0] = \frac{5c}{32}.
\end{aligned} \tag{2.5}$$

Note that the sector corresponding to the identity element  $\mathbb{1} \in S_N$  is actually the untwisted sector. As expected, this sector furnishes the true vacuum primary of weight 0.

**Symmetry structure** Consider the holomorphic and antiholomorphic Virasoro symmetry of the seed theory, collectively denoted as  $\text{Vir}(\mathcal{M})$ . The holomorphic and antiholomorphic sectors of  $\text{Vir}(\mathcal{M})$  are respectively generated by  $\{L_n^{(s)}\}$  and  $\{\bar{L}_n^{(s)}\}$ , where for a seed theory of central charge  $c$  we have

$$\begin{aligned}
[L_n^{(s)}, L_m^{(s)}] &= (n - m)L_{n+m}^{(s)} + \frac{c}{12}n(n^2 - 1)\delta_{n+m,0}, \\
[\bar{L}_n^{(s)}, \bar{L}_m^{(s)}] &= (n - m)\bar{L}_{n+m}^{(s)} + \frac{c}{12}n(n^2 - 1)\delta_{n+m,0}, \\
[L_n^{(s)}, \bar{L}_m^{(s)}] &= 0.
\end{aligned} \tag{2.6}$$

The symmetric orbifold theory  $\mathcal{M}_N$  then inherits a symmetry algebra

$$\text{Vir}(\mathcal{M})^N / S_N. \tag{2.7}$$

This contains both the holomorphic and antiholomorphic Virasoro algebras of the product theory  $\mathcal{M}^{\otimes N}$ . We refer to this subalgebra as the “full” Virasoro algebra, and we denote its holomorphic and antiholomorphic generators by  $\{L_n\}$  and  $\{\bar{L}_n\}$ , respectively. The associated stress tensor of  $\mathcal{M}^{\otimes N}$  is found by summing together the stress tensors of each copy of the seed theory. Since the product theory is non-interacting (i.e. seed Virasoro generators acting on different factors commute), the commutator of the full Virasoro generators is

$$[L_n, L_m] = \sum_{i=1}^N [L_n^{(s)}, L_m^{(s)}] \Big|_{i\text{-th copy}} = (n - m)L_{n+m} + \frac{Nc}{12}n(n^2 - 1)\delta_{n+m,0}, \tag{2.8}$$

with an equivalent expression for the antiholomorphic generators. Thus, the central charge of the full Virasoro algebra is  $Nc$ .

It is worth mentioning that (2.7) consists of more than just the full Virasoro symmetry. For example, there are also “fractional” Virasoro generators  $\{\ell_{n/k}\}$  and  $\{\bar{\ell}_{n/k}\}$  which act

only on  $k$ -twisted sectors of the theory [33, 34]. These satisfy the algebra

$$\begin{aligned} [\ell_{n/k}, \ell_{m/k}] &= \left(\frac{n-m}{k}\right) \ell_{(n+m)/k} + \frac{kc}{12} \left(\frac{n}{k}\right) \left[\left(\frac{n}{k}\right)^2 - 1\right] \delta_{n+m,0}, \\ [\bar{\ell}_{n/k}, \bar{\ell}_{m/k}] &= \left(\frac{n-m}{k}\right) \bar{\ell}_{(n+m)/k} + \frac{kc}{12} \left(\frac{n}{k}\right) \left[\left(\frac{n}{k}\right)^2 - 1\right] \delta_{n+m,0}, \\ [\ell_{n/k}, \bar{\ell}_{m/k}] &= 0. \end{aligned} \quad (2.9)$$

These are fractional modes of the part of the stress tensor obtained by summing over  $k$  copies of the seed theory [34]. They act on states in the  $k$ -twisted sector, such as bare twists or  $k$ -twisted primaries.

Twisted-sector primaries and their fractional Virasoro descendants may generically appear as terms in the boundary states of a symmetric orbifold theory. However, the boundary data with which we are concerned (the  $g$ -function and transport coefficients) do not involve these modes directly. Simply put, this data is identified as boundary-state overlaps with either the vacuum or one of its full Virasoro descendants, which live exclusively in the untwisted sector, and so twisted-sector terms are projected out. Nonetheless, fractional Virasoro generators can extract twisted-sector data encoded by a boundary state, such as transport coefficients associated with spin-2 fields besides the stress tensor [14]. We briefly elaborate in the conclusions but leave the details to future work.

## 2.2 Building the boundary states

Via folding, all physical data about a conformal interface is encoded by an associated boundary state in the closed-string spectrum of the folded BCFT [1, 2]. As such, a good starting point for studying transport coefficients in a symmetric orbifold theory is to explore how its boundary states might be written in terms of those of the seed theory. This is the goal pursued by [15]<sup>5</sup> by further focusing on boundary states which also respect particular extensions of the full Virasoro algebra inside of  $\text{Vir}(\mathcal{M})^N/S_N$ . We briefly discuss the basic idea behind the construction of [15].

**Seed boundary states** As in [15], we first suppose the seed theory  $\mathcal{M}$  has boundary states  $|b_\alpha\rangle$  where  $\alpha = 1, \dots, n_b$  is an index.  $n_b$  is either finite (for a rational seed theory) or formally infinite (for an irrational seed theory). All of these boundary states satisfy the constraint

$$\left(L_n^{(s)} - \bar{L}_{-n}^{(s)}\right) |b_\alpha\rangle = 0, \quad \forall n \in \mathbb{Z}. \quad (2.10)$$

There is a natural basis in which to write the boundary states. The solution space of (2.10) is spanned by the *Ishibashi states* of  $\mathcal{M}$  [36, 37]. Each of these is constructed from some spinless primary of weight  $h$  as follows:

$$|h\rangle\rangle = \sum_{\mathbf{m}} |h, \mathbf{m}\rangle \otimes \overline{|h, \mathbf{m}\rangle}, \quad (2.11)$$

where  $\mathbf{m}$  is either the empty set or an ordered multiset of positive integers  $(\{m_1, \dots, m_\kappa\})$  with  $i < j \implies m_i \leq m_j$ . The state  $|h, \mathbf{m}\rangle$  (resp.  $\overline{|h, \mathbf{m}\rangle}$ ) is a holomorphic (resp.

---

<sup>5</sup>See also [35] for much earlier work along these lines.

antiholomorphic) descendent of the associated primary, with the multiset labeling both the number and type of creation operators employed:<sup>6</sup>

$$\begin{aligned} |h, \{m_1, \dots, m_\kappa\}\rangle &= \left( \prod_{i=1}^{\kappa} L_{-m_i}^{(s)} \right) |h\rangle, \\ \overline{|h, \{m_1, \dots, m_\kappa\}\rangle} &= \left( \prod_{i=1}^{\kappa} \bar{L}_{-m_i}^{(s)} \right) |h\rangle. \end{aligned} \quad (2.12)$$

(2.11) defines Ishibashi states of the seed theory. All seed boundary states are linear combinations of these Ishibashi states. In the symmetric orbifold theory, we may obtain Ishibashi states built from untwisted-sector primaries by taking  $N$ -fold tensor products of (2.11) and symmetrizing. This provides a basis for untwisted states of the form

$$|B\rangle_{\text{untw}} \sim \sum_{\sigma \in S_N} |b_{\sigma(\alpha_1)}\rangle \otimes \cdots \otimes |b_{\sigma(\alpha_N)}\rangle. \quad (2.13)$$

If all  $N$  of the seed factors  $|b_{\alpha_i}\rangle$  are distinct, then the only boundary states that can be written are symmetrized product states of the form (2.13). However, we may have degenerate factors, in which case we may include twists of these seed boundary states.

**Twisting boundary states** We start by discussing twisted Ishibashi states. First, consider a  $k$ -cycle  $\sigma \in S_N$ . Prior to orbifolding, we may take a  $\sigma$ -twisted spinless primary with weight  $\sigma[h]$  (2.2) (such as the bare twist) and employ the associated fractional Virasoro generators<sup>7</sup> satisfying (2.9) to construct states

$$|\sigma[h]\rangle\rangle = \sum_{\mathbf{m}} |\sigma[h], \mathbf{m}\rangle \otimes \overline{|\sigma[h], \mathbf{m}\rangle}, \quad (2.14)$$

where this time we define

$$\begin{aligned} |\sigma[h], \{m_1, \dots, m_\kappa\}\rangle &= \left( \prod_{i=1}^{\kappa} \ell_{-m_i/k} \right) |\sigma[h]\rangle, \\ \overline{|\sigma[h], \{m_1, \dots, m_\kappa\}\rangle} &= \left( \prod_{i=1}^{\kappa} \bar{\ell}_{-m_i/k} \right) |\sigma[h]\rangle. \end{aligned} \quad (2.15)$$

By construction, the twisted Ishibashi state (2.14) satisfies

$$(\ell_{n/k} - \bar{\ell}_{-n/k}) |\sigma[h]\rangle\rangle = 0, \quad \forall n \in \mathbb{Z}. \quad (2.16)$$

We can generalize this construction to any permutation in  $S_N$ . Take  $\sigma = \sigma_1 \cdots \sigma_m \in S_N$ , where the factors  $\sigma_i$  are disjoint cycles each of length  $k_i$  and  $\sum k_i = N$  (so we are including the trivial 1-cycles). To be unambiguous, we order the factors in decreasing order in cycle

---

<sup>6</sup> $\mathbf{m} = \emptyset$  corresponds to the primary state itself.

<sup>7</sup>Here we are implicitly referring to the fractional Virasoro modes which act on the  $k$  copies of the seed theory that are glued together by  $\sigma$ .

length, i.e. we take  $k_i \geq k_{i+1}$  for all  $i = 1, \dots, m-1$ . Starting with a seed primary of weight  $h$ , we can write a corresponding twisted Ishibashi state

$$|\sigma[h]\rangle\rangle = |\sigma_1[h]\rangle\rangle \otimes \cdots \otimes |\sigma_m[h]\rangle\rangle. \quad (2.17)$$

Of course, this expression is not consistent with the permutation symmetry of the symmetric orbifold theory. We must take a symmetric sum over all cycles of the same type, which is the same as summing twisted Ishibashi states over all permutations conjugate to  $\sigma$ :

$$|\sigma[h]\rangle\rangle \longrightarrow \sum_{\substack{\sigma' \in S_N \\ \sigma' = \tau \sigma \tau^{-1}}} |\sigma'[h]\rangle\rangle. \quad (2.18)$$

This expression describes twisted Ishibashi states in all twisted sectors of the symmetric orbifold theory. To then get twisted boundary states, [15] starts with a generic seed boundary state written in the (untwisted) Ishibashi basis,

$$|b_\alpha\rangle = \sum_h \beta_{h,\alpha} |h\rangle\rangle. \quad (2.19)$$

The coefficients  $\beta_{h,\alpha}$  can then be paired with twists of the Ishibashi state  $|h\rangle\rangle$ . For a  $k$ -cycle  $\sigma$ , the associated  $\sigma$ -twisted state is

$$|\sigma \cdot b_\alpha\rangle = \sum_h \beta_{h,\alpha} |\sigma[h]\rangle\rangle. \quad (2.20)$$

For a generic permutation  $\sigma = \sigma_1 \cdots \sigma_m$  (as written above), each factor may twist a different seed boundary state, and so we get states such as

$$|\sigma \cdot b\rangle = |\sigma_1 \cdot b_{\alpha_1}\rangle \otimes \cdots \otimes |\sigma_m \cdot b_{\alpha_m}\rangle. \quad (2.21)$$

In the symmetric orbifold theory, we must once again sum over all elements conjugate to  $\sigma$ , and so a twisted-sector boundary state may contain terms of the form

$$|B\rangle_{\text{twst}} \sim \sum_{\substack{\sigma' \in S_N \\ \sigma' = \tau \sigma \tau^{-1}}} |\sigma' \cdot b\rangle. \quad (2.22)$$

[15] discusses further how (2.13) and (2.22) can be used as building blocks for a broad class of boundary states in the symmetric orbifold theory labeled by representations of permutation subgroups in  $S_N$  (where these subgroups are those which permute identical copies of seed boundary states). However, for our purposes it is sufficient to know only the general form of the boundary states—as linear combinations of (2.13) and (2.22) weighted by characters of symmetric-group representations.

### 2.3 Transport coefficients from seed data

Now, we discuss how transport coefficients [13] are encoded by the boundary states constructed from the building blocks (2.13) and (2.22). The  $g$ -function [9] has already been addressed by [15], and so we can look to the  $g$ -function for inspiration.

First, we note that the  $g$ -function is identified as the overlap between the boundary state and the vacuum  $|0\rangle^{\otimes N}$ , while transport coefficients [13] are identified with overlaps between the boundary state and full Virasoro descendants of the vacuum. Mathematically, the  $g$ -function of  $|B\rangle$  is

$$g(|B\rangle) = \langle 0|^{\otimes N} |B\rangle. \quad (2.23)$$

However, the state  $|0\rangle^{\otimes N}$  lives in the untwisted sector, and so it projects out any twisted-sector building blocks (2.22) in  $|B\rangle$ . As a result, for  $|B\rangle$  built from seed boundary states  $|b_{\alpha_1}\rangle, \dots, |b_{\alpha_N}\rangle$ , the  $g$ -function is merely the vacuum overlap with (2.13) up to an overall  $N$ -dependent normalization factor, so it is proportional to a product of seed  $g$ -functions:

$$g(|B\rangle) = \mathcal{F}(N) (g_{\alpha_1} \cdots g_{\alpha_N}), \quad g_{\alpha} = \langle 0|b_{\alpha}\rangle, \quad (2.24)$$

Now, we can discuss transport. For any 2d ICFT prior to folding, we have a “left” theory whose full Virasoro generators we write as  $\{L_i^{(L)}\}$  and  $\{\bar{L}_i^{(L)}\}$  and a “right” theory with generators  $\{L_i^{(R)}\}$  and  $\{\bar{L}_i^{(R)}\}$ . These theories also respectively have central charges  $c_L$  and  $c_R$ , respectively. Upon folding, [13] defines a  $2 \times 2$  “transport matrix”

$$R_{IJ}(|B\rangle) = \frac{\langle \Omega | L_2^{(I)} \bar{L}_2^{(J)} | B \rangle}{\langle \Omega | B \rangle}, \quad I, J = L, R, \quad (2.25)$$

where we use  $|\Omega\rangle$  to represent the vacuum of the folded theory. In terms of the transport matrix, the energy transmission and reflection coefficients may be written as

$$\mathcal{T} = \frac{2}{c_L + c_R} (R_{LR} + R_{RL}), \quad \mathcal{R} = \frac{2}{c_L + c_R} (R_{LL} + R_{RR}). \quad (2.26)$$

Furthermore, the analogous matrices to (2.25) defined with higher-level Virasoro modes do not give additional information; they are simply proportional to (2.25) [13].

We now write (2.25) in a generic symmetric orbifold theory at the orbifold point. First, recall that the  $n$ th full Virasoro generator is a sum over  $n$ th Virasoro generators of each copy of the seed theory. So, we have that

$$L_2^{(I)} \bar{L}_2^{(J)} = \left( \sum_{i=1}^N L_2^{(s)(I)} \Big|_{i\text{-th copy}} \right) \left( \sum_{j=1}^N \bar{L}_2^{(s)(J)} \Big|_{j\text{-th copy}} \right). \quad (2.27)$$

However, when inserted between the vacuum  $\langle 0|^{\otimes N}$  and a boundary state  $|B\rangle$ , any “cross terms” formed by a product of Virasoro modes acting on different copies of the seed theory are annihilated. This is because, on a single copy, we can use the condition (2.10) to write

$$\langle 0 | L_2^{(s)} | b_{\alpha} \rangle = \langle 0 | \bar{L}_2^{(s)} | b_{\alpha} \rangle = \left( \bar{L}_2^{(s)} | 0 \rangle \right)^{\dagger} | b_{\alpha} \rangle = 0, \quad (2.28)$$

and similarly for  $\langle 0 | \bar{L}_2^{(s)} | b_{\alpha} \rangle$ . Thus, we can write the numerator of the transport matrix as

$$\langle 0|^{\otimes N} L_2^{(I)} \bar{L}_2^{(J)} | B \rangle = \langle 0|^{\otimes N} | B \rangle \sum_{i=1}^N \frac{\langle 0 | L_2^{(s)(I)} \bar{L}_2^{(s)(J)} | b_{\alpha_i} \rangle}{\langle 0 | b_{\alpha_i} \rangle}, \quad (2.29)$$

and as a result we have that the transport matrix at the orbifold point of the symmetric orbifold theory is a sum of transport matrices associated with the seed boundary states:

$$R_{IJ}(|B\rangle) = \sum_{i=1}^N R_{IJ}(|b_{\alpha_i}\rangle). \quad (2.30)$$

Note that there is no combinatorial factor here. This is because the numerator of the transport matrix is normalized by the  $g$ -function of  $|B\rangle$ .

Now, denote the transmission and reflection coefficients associated with the boundary state  $|b_{\alpha_i}\rangle$  by  $\mathcal{T}_{\alpha_i}$  and  $\mathcal{R}_{\alpha_i}$ , respectively. Furthermore, recall  $c_L = Nc_L^{(s)}$  and  $c_R = Nc_R^{(s)}$ , where  $c_L^{(s)}$  and  $c_R^{(s)}$  are respectively the central charges of the left and right seed theories. From (2.26), we have that the transmission and reflection coefficients encoded by  $|B\rangle$  are

$$\mathcal{T}(|B\rangle) = \frac{2}{Nc_L^{(s)} + Nc_R^{(s)}} \sum_{i=1}^N [R_{LR}(|b_{\alpha_i}\rangle) + R_{RL}(|b_{\alpha_i}\rangle)] = \frac{1}{N} \sum_{i=1}^N \mathcal{T}_{\alpha_i}, \quad (2.31)$$

$$\mathcal{R}(|B\rangle) = \frac{2}{Nc_L^{(s)} + Nc_R^{(s)}} \sum_{i=1}^N [R_{LL}(|b_{\alpha_i}\rangle) + R_{RR}(|b_{\alpha_i}\rangle)] = \frac{1}{N} \sum_{i=1}^N \mathcal{R}_{\alpha_i}. \quad (2.32)$$

In other words, the transport coefficients encoded by some boundary state  $|B\rangle$  is an average of the transport coefficients of each individual seed boundary state in  $|B\rangle$ . As a consistency check, observe that the transport coefficients indeed sum to 1 if each  $\mathcal{T}_{\alpha_i} + \mathcal{R}_{\alpha_i} = 1$ .

A brief caveat—it is worth noting that the transport coefficients here are strictly associated with excited states created by the full stress tensor. Because symmetric orbifold theories have more than just Virasoro symmetry, one expects the presence of other spin-2 quasi-primary operators whose modes reside in the extended symmetry algebra (possibly described by particular combinations of fractional Virasoro modes). As discussed by [14], the states created by these operators furnish their own independent transport coefficients.

Lastly, we reiterate that we have assumed the  $N$  copies of the seed theory do not interact in obtaining our result. As such, it is only expected to hold at the orbifold point. In the strongly coupled regime far from the orbifold fixed point, mixing between the different copies would spoil the decomposition of the transport matrix (2.30). One known way to access this sector is through holography, as we discuss next.

### 3 The holographic symmetric orbifold of the $\mathbb{T}^4$ ICFT

As a particularly tractable example, we examine transport in the symmetric orbifold of an ICFT represented by a  $\mathbb{T}^4$  sigma model. The seed ICFT consists of four copies of a scalar field  $\tilde{\phi} : \mathbb{R} \rightarrow S^1$  which “jumps” in coupling at some interface. To approximate the weakly coupled regime, we take the seed theory to consist of free scalars described by the action

$$I_{S^1} = \frac{R_-^2}{2} \int_{\tilde{y} < 0} dt d\tilde{y} (\partial \tilde{\phi}_-)^2 + \frac{R_+^2}{2} \int_{\tilde{y} > 0} dt d\tilde{y} (\partial \tilde{\phi}_+)^2. \quad (3.1)$$

The couplings  $R_{\pm}$  are the radii of the target space on the two sides of the interface.<sup>8</sup>

---

<sup>8</sup>Note that we are assuming the target space to be a square torus, with all of the radii equal.

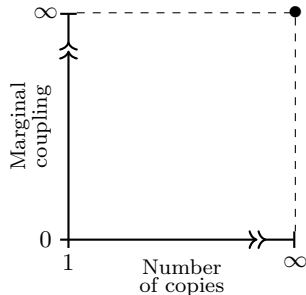


**Figure 3:** The parameter space of the symmetric orbifold of  $\mathbb{T}^4$ . We can dial both the number of seed copies and the marginal coupling which makes the copies interact. The bottom axis (with coupling = 0) describes the orbifold point. The black point is the holographic limit at which the description by type IIB supergravity on Janus is valid.

The strongly coupled, large- $N$  regime of the symmetric orbifold theory is described by type IIB supergravity on 3-dimensional Janus [24] (Figure 3). This background is a solution to the type IIB supergravity action constructed by deforming the  $\text{AdS}_3 \times S^3 \times \mathbb{T}^4$  vacuum with a dilaton. 3d Janus is under a large amount of analytic control, just like the thin-brane models used in previous studies of holographic interfaces [25, 26, 38, 39].

It is possible to compute transport coefficients in the strongly coupled regime for the interface described by the Janus solution through recently developed methods [26, 27]. Additionally, working directly in pure Janus specifies a particular boundary state on the field-theory side constructed from copies of the same seed boundary state [12, 23]. With this in mind, we can also approximate the associated transport coefficients in the weakly coupled regime because the free-scalar seed theory (3.1) is rather simple (cf. [13]). Upon doing so, we compare the answer against that of [27] to bound the running of transport coefficients in the marginal coupling of the ICFT.

### 3.1 3d Janus and holography

**Gravitational solution** In the Einstein frame of the type IIB supergravity action, we consider solutions of the form

$$ds_{\text{IIB}}^2 = e^{\phi/2} (ds_3^2 + d\Omega_3^2)^2 + e^{-\phi/2} ds_{\mathbb{T}^4}^2. \quad (3.2)$$

The dimensional reduction of the action onto the 3 noncompact dimensions is

$$S_{\text{GR}}^{(3)}[g, \phi] = \frac{1}{16\pi G_N^{(3)}} \int d^3x \sqrt{-g} \left( R + \frac{2}{L^2} - \partial_\alpha \phi \partial^\alpha \phi \right), \quad (3.3)$$

where  $G_N^{(3)}$  is the 3d Newtonian constant,  $L$  is a length scale, and Greek indices run over spacetime. The classical equations of motion are

$$G_{\mu\nu} - \frac{1}{L^2} g_{\mu\nu} = \partial_\mu \phi \partial_\nu \phi - \frac{g_{\mu\nu}}{2} \partial_\alpha \phi \partial^\alpha \phi, \quad (3.4)$$

$$\nabla_\mu \nabla^\mu \phi = 0. \quad (3.5)$$

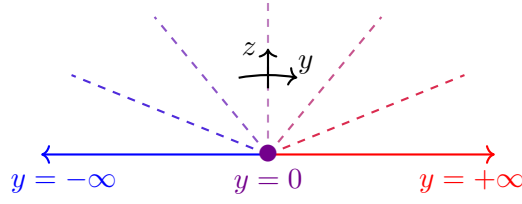


**Figure 4:** A constant-time slice of 3-dimensional Janus with radial coordinate  $z$  and hyperbolic angular coordinate  $y$ . The dashed lines are  $\text{AdS}_2$  slices of the bulk. The  $y = 0$  point is the interface between the left ( $y < 0$ ) and right ( $y > 0$ ) CFTs.

For the 3d spacetime, we assume the ansatz

$$\frac{ds^2}{L^2} = \frac{f(y)}{z^2}(-dt^2 + dz^2) + dy^2, \quad \phi = \phi(y), \quad (3.6)$$

with  $t, y \in (-\infty, \infty)$  and  $z > 0$ . The 3d Janus solution corresponds to the metric function,

$$f(y) = \frac{1}{2} \left[ 1 + \sqrt{1 - 2\gamma^2} \cosh(2y) \right], \quad (3.7)$$

where  $\gamma \in \left[0, \frac{1}{\sqrt{2}}\right)$  is some parameter characterizing the solution.<sup>9</sup> See Figure 4 for a visual representation of 3d Janus. In this background, the dilaton's profile is

$$\phi(y) = \phi_0 + \frac{1}{\sqrt{2}} \log \left( \frac{1 + \sqrt{1 - 2\gamma^2} + \sqrt{2}\gamma \tanh y}{1 + \sqrt{1 - 2\gamma^2} - \sqrt{2}\gamma \tanh y} \right), \quad (3.8)$$

Thus, the asymptotic values of the dilaton are

$$\phi_{\pm} = \lim_{y \rightarrow \pm\infty} \phi(y) = \phi_0 \pm \frac{1}{2\sqrt{2}} \log \left( \frac{1 + \sqrt{2}\gamma}{1 - \sqrt{2}\gamma} \right). \quad (3.9)$$

One benefit of studying the 3d Janus solution is that the dual field theory is known to be a highly deformed (i.e. strongly coupled) symmetric orbifold ICFT. The parameters of the theory can be described in terms of the number of fundamental D-branes.

**Field-theory dual** The starting point is to recall the holographic dual of type IIB string theory on  $\text{AdS}_3 \times S^3 \times \mathbb{T}^4$ . There, we take the D1/D5 system consisting of  $Q_1$  D1-branes and  $Q_5$  D5-branes in  $\mathbb{R}^6 \times \mathbb{T}^4$  [40]. For large  $Q_1, Q_5 \gg \frac{1}{g_s} \gg 1$ , the AdS/CFT correspondence describes a duality between type IIB supergravity on  $\text{AdS}_3 \times S^3 \times \mathbb{T}^4$  and a strongly coupled CFT on the boundary of  $\text{AdS}_3 \times S^3$ . The target space of the CFT is topologically  $(\mathbb{T}^4)^{Q_1 Q_5} / S_{Q_1 Q_5}$  [20, 41, 42], and so it is a highly deformed symmetric orbifold theory consisting of  $N = Q_1 Q_5 \gg 1$  copies of a  $\mathbb{T}^4$  sigma model.

To construct the Janus solution, we are adding a (non-supersymmetric) dilatonic deformation on top of the  $\text{AdS}_3 \times S^3 \times \mathbb{T}^4$  vacuum. As this dilaton asymptotes to two distinct values on the AdS boundary (3.9), the bulk deformation introduces an interface in the dual symmetric orbifold theory.

<sup>9</sup> $\gamma = 0$  corresponds to the non-deformed  $\text{AdS}_3$  vacuum, and we find naked singularities if  $\gamma^2 > \frac{1}{2}$  [24].

We can identify the radius of each  $S^1$  factor of the target-space torus with the asymptotic value of  $e^{-\phi/2}$  [12]. However, since the dilaton profile (3.8) takes two values at infinity (3.9), the radius “jumps” between two values  $R_+$  and  $R_-$ , where

$$R_{\pm} \sim e^{-\phi_{\pm}/2} = e^{-\phi_0/2} \left( \frac{1 + \sqrt{2}\gamma}{1 - \sqrt{2}\gamma} \right)^{\mp \frac{1}{4\sqrt{2}}}. \quad (3.10)$$

We interpret this nontrivial jump as describing the presence of an interface in the theory. With this in mind, observe that the ratio of the two radii,

$$\frac{R_+}{R_-} = \left( \frac{1 + \sqrt{2}\gamma}{1 - \sqrt{2}\gamma} \right)^{-\frac{1}{2\sqrt{2}}}, \quad (3.11)$$

goes to 1 as  $\gamma \rightarrow 0$  (the interface disappears) and goes to 0 as  $\gamma \rightarrow \frac{1}{\sqrt{2}}$  (there is a parametrically large separation of scales between the sides). Intuitively, we expect these limits to respectively correspond to a completely transparent or completely reflective interface.

Note that the form of the boundary state encoding the Janus interface is not obvious. However, [12] finds it to consist of  $N$  identical copies of a four-fold “Neumann–Dirichlet” state in the  $\mathbb{T}^4$  sigma model. Each Neumann–Dirichlet describes a boundary state of one of the  $S^1$  factors. While there may be twisted-sector terms, our analysis of transport is not sensitive to the resulting combinatorial factors and does not probe such terms.

### 3.2 Strong-coupling transport from gravity waves

The basic idea of [25] for computing transport coefficients is to consider linearized, source-free fluctuations of the metric in Fefferman–Graham (FG) gauge [43] (setting  $L = 1$ ),

$$ds_{\text{FG}}^2 = \frac{du^2}{u^2} + \frac{1}{u^2} \left[ g_{ij}^{(0)} + u^2 g_{ij}^{(2)} + \frac{u^4}{4} g_{ij}^{(4)} + \dots \right] dw^i dw^j, \quad (3.12)$$

where  $u > 0$  is the radial coordinate and the Latin indices run over the remaining  $1 + 1$  dimensions. These fluctuations are called *surface gravity waves*, and in the boundary theory they corresponds to excitations produced by the stress tensor [43, 44]. In the thin-brane model of [25] consisting of two  $\text{AdS}_3$  geometries glued along an  $\text{AdS}_2$  surface, we scatter these surface gravity waves off of the brane. This corresponds to the scattering *gedankenexperiment* of [14] in the boundary theory. The amplitudes of the reflected and transmitted waves can be translated into the transport coefficients. The bulk equations of motion and boundary conditions can then be used to constrain these transport coefficients.

**Scattering on Janus** We may attempt an analogous scattering experiment directly in Janus. While possible in principle, this is difficult in practice. To see why, we first write (3.6) in FG form to serve as the background of our scattering experiment. This has been done perturbatively in the Janus parameter by [45] (see also [46, 47]). Up to the first subleading term of order  $\gamma^2$ , we approximate the metric function  $f$  in (3.6) as

$$f(y) = \cosh^2 y - \frac{1}{2} \gamma^2 \cosh^2 y + O(\gamma^4). \quad (3.13)$$

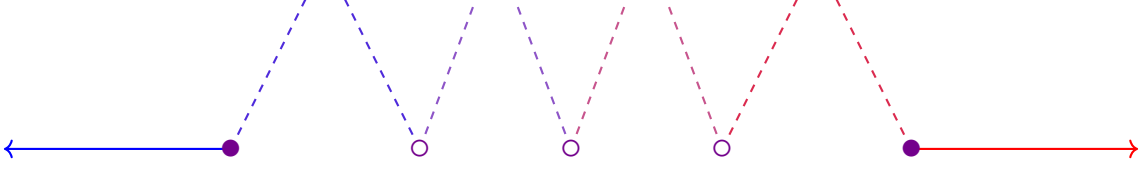


**Figure 5:** A discrete array of thin branes in  $\text{AdS}_3$ . This is the setup used by [26] to extend the prescription for transport coefficients of [25] beyond the case of a thin brane with one tension parameter. “Thick brane” configurations in which the interface is represented by a smooth geometry foliated into AdS slices can be discretized into an array of thin branes.

Taking  $\gamma = 0$  (pure AdS), the FG metric comes about through the coordinate transformation  $z \rightarrow \sqrt{\tilde{y}^2 + u^2}$  and  $y \rightarrow \text{Sinh}^{-1}\left(\frac{\tilde{y}}{u}\right)$ . For Janus, we thus consider the ansatz

$$z \rightarrow \sqrt{\tilde{y}^2 + u^2} + \gamma^2 u f_z\left(\frac{\tilde{y}}{u}\right) + O(\gamma^4), \quad y \rightarrow \text{Sinh}^{-1}\left(\frac{\tilde{y}}{u}\right) + \gamma^2 f_y\left(\frac{\tilde{y}}{u}\right) + O(\gamma^4). \quad (3.14)$$

Upon plugging this in and insisting that the geometry is still asymptotically AdS (as  $u \rightarrow 0$ ), we find the functions

$$f_z(x) = \frac{-2 + (1 + 2x^2) \log\left(\frac{1+x^2}{x^2}\right)}{8\sqrt{1+x^2}}, \quad f_y(x) = \frac{1 + 4x^2 + x^2 \log\left(\frac{1+x^2}{x^2}\right)}{8x\sqrt{1+x^2}}, \quad (3.15)$$

for which the transformed metric truncated at order  $\gamma^2$  is<sup>10</sup>

$$\begin{aligned} ds^2 &\sim \frac{du^2}{u^2} - \left[ \frac{1}{u^2} + \frac{\gamma^2}{4} \left( \frac{1}{u^2 + \tilde{y}^2} - \frac{1}{u^2} \log\left(1 + \frac{u^2}{\tilde{y}^2}\right) \right) \right] dt^2 \\ &\quad + \left[ \frac{1}{u^2} - \frac{\gamma^2}{4} \left( \frac{1}{\tilde{y}^2} - \frac{1}{u^2} \log\left(1 + \frac{u^2}{\tilde{y}^2}\right) \right) \right] d\tilde{y}^2 \\ &= \frac{du^2}{u^2} + \frac{1}{u^2} \left[ (-dt^2 + d\tilde{y}^2) - \frac{u^4}{4} \frac{\gamma^2}{2\tilde{y}^4} (-dt^2 + d\tilde{y}^2) + \dots \right]. \end{aligned} \quad (3.16)$$

Unlike the thin-brane solution on  $\text{AdS}_3$  used by [25], the metric does not truncate at the  $g_{ij}^{(4)}$  term. As a matter of practicality, this makes it difficult to compute constraints from fluctuations on Janus even up to order- $\gamma^2$  terms. Additionally, the fluctuations may themselves need  $\gamma$ -dependence in order for the constraints to be nontrivial.

Most importantly, our goal is to perform a strong-weak comparison over the full range of the Janus parameter  $\gamma$ . As such, while a perturbative calculation might be a useful proof of principle, it is not particularly helpful in accomplishing our ultimate purpose.

**Stacking branes** Fortunately, a different  $\gamma$ -exact calculation of the transport coefficients in 3d Janus has been performed by [27]. The first step had been taken by [26], which extended the earlier thin-brane method to “arrays” of thin branes (Figure 5). This provides more parametric freedom in the bulk and allows for holographic computations of transport coefficients encoded by a broader class of interfaces.

<sup>10</sup>The transformation (3.14) induces terms which are  $O(\gamma^4)$ , but we omit these terms.

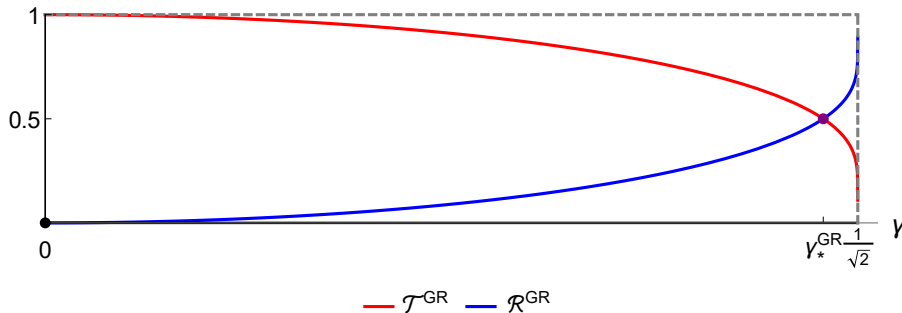


**Figure 6:** The transmission (red) and reflection (blue) coefficients of the Janus boundary state computed from holography, plotted as functions of the Janus parameter  $\gamma \in \left[0, \frac{1}{\sqrt{2}}\right)$ . For small  $\gamma$ , the transmission coefficient is near 1, which is consistent with the interface disappearing at  $\gamma = 0$ . For large  $\gamma$ , the reflection coefficient goes to 1, which is consistent with the jump becoming infinite at  $\gamma = \frac{1}{\sqrt{2}}$ . The purple point designates the value for which  $\mathcal{T}^{\text{GR}} = \mathcal{R}^{\text{GR}}$ . This happens at  $\gamma = \gamma_*^{\text{GR}} \approx 0.677$ .

[27] considers interfaces which are holographically described by continuous  $(d+1)$ -dimensional bulk geometries that can be foliated into  $\text{AdS}_d$  slices, such as the Janus solution. They observe that these “thick-brane” geometries can be treated as a limit of a discrete array of thin branes. For 3d Janus<sup>11</sup> in particular, they find a tension “density” for the branes in this array and integrate to compute an “effective” tension. Plugging this into the original thin-brane formula [25] yields a  $\gamma$ -exact holographic transmission coefficient:

$$\mathcal{T}^{\text{GR}} = \frac{\sqrt{2}\gamma}{\text{Tanh}^{-1}(\sqrt{2}\gamma)} = 1 - \frac{2}{3}\gamma^2 - \frac{16}{45}\gamma^4 + O(\gamma^6). \quad (3.17)$$

This is expected to be equivalent to the answer obtained by scattering surface gravity waves directly on Janus. Nonetheless, this approach is much less tedious and more powerful.

It is worth comparing the Janus result against that of the thin-brane models [25]. In the latter, the underlying action is Einstein plus a Randall–Sundrum term [48, 49]. The tension is thus an effective coupling constant, and tuning the transport coefficients requires fixing the tensions by hand—a fine-tuning problem. However, 3d Janus is a genuine top-down solution, and so we should not require fine-tuning to achieve a particular  $\mathcal{T}$  and  $\mathcal{R}$ . Indeed, the Janus parameter  $\gamma$  is an integration constant labeling the solutions rather than a coupling, and the full physical range of  $\gamma$  furnishes all values for the transport coefficients.

We conclude by plotting the holographic transport coefficients against one another (noting  $\mathcal{R}^{\text{GR}} = 1 - \mathcal{T}^{\text{GR}}$ ) in Figure 6. As anticipated in Section 3.1,  $\gamma = 0$  corresponds a maximally transmissive interface, while  $\gamma = \frac{1}{\sqrt{2}}$  describes a maximally reflective interface. Observe that there is a distinguished value of  $\gamma$  at which the transport coefficients match:

$$\gamma_*^{\text{GR}} \approx 0.677. \quad (3.18)$$

<sup>11</sup>[27] uses a slightly different Janus parameter. We present their result in terms of  $\gamma$ .

### 3.3 Weak-coupling transport from seed theory

We now calculate the transport coefficients in the free sector of the  $\mathbb{T}^4$  symmetric orbifold ICFT. As we are at the orbifold point, we only need the transport coefficients of the individual seed boundary states used to construct the Janus interface. Then, just as in [12], we take  $4N = 4Q_1Q_5$  copies of the Neumann–Dirichlet state in the free scalar theory. With the seed coefficients in hand, we then employ the prescription of Section 2—namely (2.31)–(2.32)—to write the “full” transport coefficients.

The seed theory consists of four copies of a free scalar field on 2d Minkowski spacetime  $-dt^2 + d\tilde{y}^2$  whose target space is  $S^1$  and with an interface at  $\tilde{y} = 0$ :

$$S_{\text{FT}}[\tilde{\phi}] = \frac{R_-^2}{2} \int_{\tilde{y} < 0} dt d\tilde{y} \partial_i \tilde{\phi}_- \partial^i \tilde{\phi}_- + \frac{R_+^2}{2} \int_{\tilde{y} > 0} dt d\tilde{y} \partial_i \tilde{\phi}_+ \partial^i \tilde{\phi}_+, \quad (3.19)$$

where  $i$  here is a spacetime index running over  $(t, \tilde{y})$ .

The transmission and reflection coefficients in this  $S^1$  theory have been computed by [13] (based on [50]). For now, we simply need to recast their results in terms of  $R_{\pm}$ . To complete this exercise, we require the behavior of the fields at the interface. Reintroducing coordinate dependence as  $\tilde{\phi} \rightarrow \tilde{\phi}(t, \tilde{y})$ , we demand  $\delta\tilde{\phi}_+(t, 0) = \delta\tilde{\phi}_-(t, 0)$  [12]. By varying the action and integrating by parts, we then get the boundary condition at  $\tilde{y} = 0$ :

$$R_+^2 \partial_{\tilde{y}} \tilde{\phi}_+ = R_-^2 \partial_{\tilde{y}} \tilde{\phi}_-. \quad (3.20)$$

This can be rewritten as a matrix equation in the form presented by [13]. Identifying  $\pm \partial_{\tilde{y}} \leftrightarrow \partial_{\pm}$ , we write

$$\begin{pmatrix} \partial_- \tilde{\phi}_- \\ \partial_+ \tilde{\phi}_+ \end{pmatrix} = S \begin{pmatrix} \partial_+ \tilde{\phi}_- \\ \partial_- \tilde{\phi}_+ \end{pmatrix}, \quad S = \begin{pmatrix} -\cos(2\theta) & \sin(2\theta) \\ \sin(2\theta) & \cos(2\theta) \end{pmatrix}, \quad (3.21)$$

where we have identified

$$\cos(2\theta) = 1 - \frac{2R_-^4}{R_+^4 + R_-^4}, \quad \sin(2\theta) = \frac{2R_+^2 R_-^2}{R_+^4 + R_-^4}. \quad (3.22)$$

The transmission and reflection coefficients in the free theory on  $S^1$  are then

$$\mathcal{T}_{S^1}^{\text{FT}} = \sin^2(2\theta) = \frac{4}{\left[ \left( \frac{R_+}{R_-} \right)^2 + \left( \frac{R_-}{R_+} \right)^2 \right]^2}, \quad (3.23)$$

$$\mathcal{R}_{S^1}^{\text{FT}} = \cos^2(2\theta) = \frac{\left[ \left( \frac{R_+}{R_-} \right)^2 - \left( \frac{R_-}{R_+} \right)^2 \right]^2}{\left[ \left( \frac{R_+}{R_-} \right)^2 + \left( \frac{R_-}{R_+} \right)^2 \right]^2}. \quad (3.24)$$

The seed  $\mathbb{T}^4$  sigma model consists of four non-interacting  $S^1$  factors. For boundary states in the product theory, a similar argument to that of a symmetric orbifold theory at the orbifold point (Section 2.3) applies; the transport coefficients of a product state are averages of the transport coefficients of the individual factors (2.31)–(2.32). As the  $S^1$  factors have

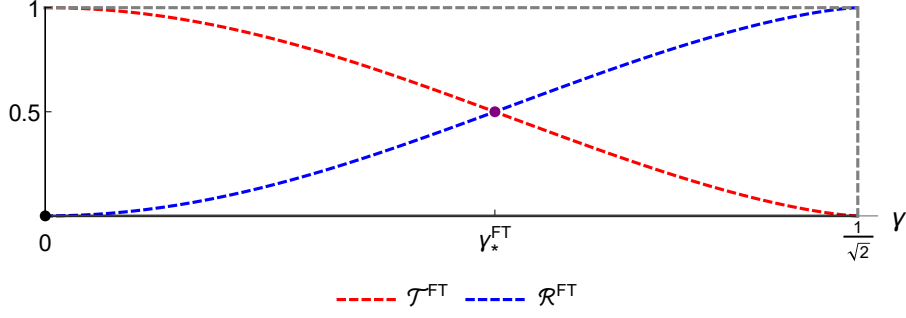


**Figure 7:** The transmission (red) and reflection (blue) coefficients of the Janus boundary state at the orbifold point as functions of the Janus parameter  $\gamma \in \left[0, \frac{1}{\sqrt{2}}\right)$ . As with the holographic coefficients, we have a  $\mathcal{T} \approx 1$  for small  $\gamma$  and  $\mathcal{R} \approx 1$  for large  $\gamma$ . The purple point is where  $\mathcal{T}^{\text{FT}} = \mathcal{R}^{\text{FT}}$ , which happens at  $\gamma = \gamma_*^{\text{FT}} \approx 0.391$ .

the same boundary condition, we deduce that the transmission and reflection coefficients in the  $\mathbb{T}^4$  theory are still given by (3.23)–(3.24). Furthermore, as all of the seed boundary states are also identical, the total transmission and reflection coefficients (respectively  $\mathcal{T}^{\text{FT}}$  and  $\mathcal{R}^{\text{FT}}$ ) are simply the seed values, because they too are computed as averages.

Now, we may recast the transport coefficients in terms of the Janus parameter  $\gamma$  using (3.11). Doing so for the transmission coefficient  $\mathcal{T}^{\text{FT}}$ , we have that

$$\mathcal{T}^{\text{FT}} = \frac{4(1 + \sqrt{2}\gamma)^{\sqrt{2}}(1 - \sqrt{2}\gamma)^{\sqrt{2}}}{\left[(1 + \sqrt{2}\gamma)^{\sqrt{2}} + (1 - \sqrt{2}\gamma)^{\sqrt{2}}\right]^2} = 1 - 4\gamma^2 + \frac{16}{3}\gamma^4 + O(\gamma^6). \quad (3.25)$$

It is also illustrative to plot both transport coefficients as functions of  $\gamma$  (Figure 7). The behaviors of  $\mathcal{T}^{\text{FT}}$  and  $\mathcal{R}^{\text{FT}}$  in the  $\gamma \rightarrow 0$  and  $\gamma \rightarrow \frac{1}{\sqrt{2}}$  limits are consistent with the intuition expressed in Section 3.1. Furthermore, the  $\gamma$  for which the coefficients are the same is

$$\gamma_*^{\text{FT}} = \frac{1}{\sqrt{2}} \tanh \left[ \frac{1}{\sqrt{2}} \log(1 + \sqrt{2}) \right] \approx 0.391. \quad (3.26)$$

### 3.4 Comparing across regimes

Equipped with the transport coefficients of the Janus interface both at strong and weak coupling, we now compare the results. To reiterate, the strong-coupling transmission coefficient is approximately the answer obtained from the Janus solution,

$$\mathcal{T}_{\text{strong}} \sim \frac{\sqrt{2}\gamma}{\text{Tanh}^{-1}(\sqrt{2}\gamma)} = 1 - \frac{2}{3}\gamma^2 - \frac{16}{45}\gamma^4 + O(\gamma^6), \quad (3.27)$$

while the weak-coupling transmission coefficient is approximately the one computed directly from the  $\mathbb{T}^4$  symmetric orbifold theory at the orbifold point,

$$\mathcal{T}_{\text{weak}} \sim \frac{4(1 + \sqrt{2}\gamma)^{\sqrt{2}}(1 - \sqrt{2}\gamma)^{\sqrt{2}}}{\left[(1 + \sqrt{2}\gamma)^{\sqrt{2}} + (1 - \sqrt{2}\gamma)^{\sqrt{2}}\right]^2} = 1 - 4\gamma^2 + \frac{16}{3}\gamma^4 + O(\gamma^6). \quad (3.28)$$

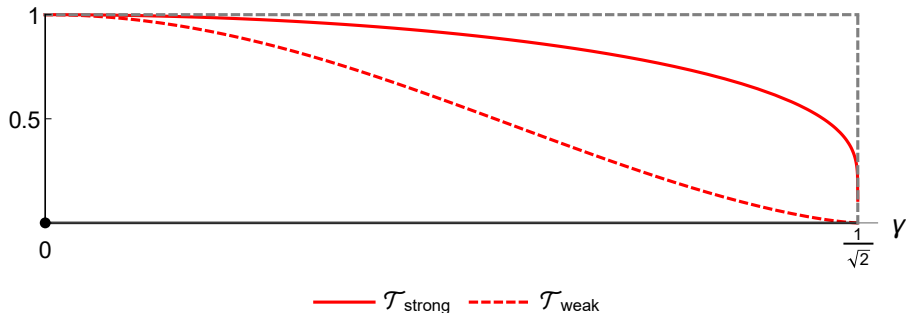


**Figure 8:** The transmission coefficients as functions of the Janus parameter  $\gamma \in \left[0, \frac{1}{\sqrt{2}}\right)$  both at strong coupling (solid) and at weak coupling (dashed). While they match at the extremal values of  $\gamma$ , the values at strong coupling are consistently larger than those at weak coupling. Furthermore, the weak-coupling coefficient has an inflection point at  $\gamma \approx 0.406$ , whereas the strong-coupling coefficient has a strictly negative derivative.

These are both plotted in Figure 8.

We immediately observe that  $\mathcal{T}_{\text{strong}} > \mathcal{T}_{\text{weak}}$  away from the extremal values of  $\gamma$ . In other words, turning on the marginal coupling which deforms the symmetric orbifold theory also increases the proportion of energy transmitted through the interface at fixed  $\gamma$ . This makes intuitive sense—energy is able to be exchanged between different copies of the seed left and right CFTs, whereas at the orbifold point these copies do not interact at all. Furthermore, this is consistent with the Janus parameter for which  $\mathcal{T} = \mathcal{R}$  being much larger for the holographic calculation (3.18) than for the field-theoretic calculation (3.26).

We also observe that the two functions are structurally different. While  $\mathcal{T}_{\text{strong}}(\gamma)$  has a strictly negative derivative and approaches 0 rapidly,  $\mathcal{T}_{\text{weak}}(\gamma)$  has an inflection point at  $\gamma \approx 0.406$  and approaches 0 more slowly. This indicates that the functional form of transmission changes as the coupling runs. This is very different from the situation for boundary entropy [12, 23], in which the analogous strong-weak comparison involves rather similar functions of  $\gamma$ .

## 4 Discussion

To summarize, we have first explored transport coefficients of interfaces in generic symmetric orbifold theories (taken at their orbifold points). In particular, we have used BCFT techniques to write them in terms of “seed” transport coefficients, using the boundary-state construction of [15] and applying the approach of [13]. We have found that, regardless of the number of copies  $N$ , the transport coefficients of the boundary states in a symmetric orbifold theory are averages of transport coefficients encoded by seed-theory boundary states, as per the formulas (2.31)–(2.32).

The second part of this paper is a study of the  $\mathbb{T}^4$  symmetric orbifold theory. This theory can be understood at strong marginal coupling (away from the orbifold point) through the AdS/CFT correspondence. A simple class of interfaces in this theory are

described by the 3d Janus solution to type IIB supergravity [24]. From the tools of gravity, one can extract transport coefficients for this class of interfaces at strong coupling [27]. Furthermore, we compute the transport coefficients at weak coupling (at the orbifold point) by combining our earlier methods and with our knowledge of the seed  $\mathbb{T}^4$  sigma model.

This sets the stage for a comparison between the transport coefficients at strong coupling and at weak coupling for Janus interfaces in the symmetric orbifold of  $\mathbb{T}^4$ . We ultimately find a significant, lawful difference. The coefficients are structurally different functions of  $\gamma$ , but transmission through the interface is larger at large coupling.

#### 4.1 Transport versus thermodynamics

Our final result in the symmetric orbifold of  $\mathbb{T}^4$  is notably different from previous analogous computations of the boundary entropy [12, 23]. In those cases, boundary entropy of the Janus interface had been found to be relatively protected from the running of the coupling, with supersymmetry *completely* protecting it [23]. Meanwhile, the transport coefficients develop different functional features entirely—most notably the loss of the inflection point at strong coupling in Figure 8.

This is reasonable in light of other strong-weak comparisons in holography. One can look to the case of  $\mathcal{N} = 4$  4d supersymmetric Yang–Mills (SYM) theory, which at strong ’t Hooft coupling is dual to type IIB supergravity on  $\text{AdS}_5 \times S^5$ . There, the free energy, which like boundary entropy is a thermodynamic quantity, has been computed both in the free theory and at strong coupling through holography [28, 29]. While the coupling runs over an infinite range, the free energy only changes by a finite factor of  $\frac{3}{4}$ .

Another quantity which has been compared at both regimes is the shear viscosity of the SYM plasma [30–32]. This quantity is associated with transport, and its story is very different from that of the free energy. In units of entropy density, it is well-known that the shear viscosity reaches a finite value of  $\frac{1}{4\pi}$  at strong coupling. However, it blows up at weak coupling. Thus, the functional dependence on coupling is not described by a finite interpolating function, unlike for free energy.

Of course, we are comparing different quantities—the boundary entropy versus the transmission coefficient—from those of the  $\mathcal{N} = 4$  SYM story. However, they are still respectively facets of thermodynamics and transport, and we again see that the thermodynamic quantity (boundary entropy) is much more strongly [12] (or even completely [23]) protected from the running of the coupling than the transport quantity (transmission coefficient). It would thus be interesting to further scrutinize the validity of this idea that “transport rushes as thermodynamics dawdles” in coupling, with Janus setups (including the higher-dimensional version [51, 52]) being a realm for doing so.

#### 4.2 The Janus boundary state

We emphasize that the specific form of the boundary state encoding a Janus interface is not obvious. To glean some insight, we look to the holographic calculation of the boundary entropy in [12] and assume that this should be (reasonably) protected from the running of

the marginal coupling. Employing the Ryu–Takayanagi formula [53] yields

$$S_b^{\text{GR}} = N \log \left( \frac{1}{\sqrt{1 - 2\gamma^2}} \right), \quad N = Q_1 Q_5 \gg 1. \quad (4.1)$$

From this, we glean that boundary entropy is an order- $N$  quantity at large  $N$ . Furthermore, in performing their comparison with the value at the orbifold point, [12] finds and uses the fact that all copies of the seed boundary state are identical—they are 4-fold products of a “Neumann-Dirichlet” boundary state in the  $S^1$  theory  $|b_{\text{ND}}\rangle$ .

However, this is not enough to specify the form of the boundary state  $|B_J\rangle$ . For example, we can imagine that it takes the form

$$|B_J\rangle = \left( |b_{\text{ND}}\rangle^{\otimes 4} \right)^{\otimes N}. \quad (4.2)$$

This is assumed by [12, 23] in computing boundary entropy at the orbifold point. In support of this, a lack of twisted-sector terms is not unreasonable. Janus is a type IIB supergravity vacuum. The density of states (in scaling dimension) of the ICFT dual to supergravity on Janus should obey supergravity-like (slow) growth (cf. [54, 55]). Twisted sectors in the symmetric orbifold theory, however, obey Hagedorn (fast) growth at large  $N$  [56]. As such, we might only expect to get an interface consistent with the Janus solution if we omit twisted-sector terms.

Another option is to posit the presence of twisted-sector terms, i.e. that the boundary state encoding the Janus interface is built from building blocks (2.13) and (2.22) obtained from a  $\mathbb{T}^4$  seed theory. Note however that this state should not describe a “typical” interface in the symmetric orbifold of  $\mathbb{T}^4$  [15]. A more typical state would be built from all distinct seed states (rather than  $N$  copies of  $|b_{\text{ND}}\rangle^{\otimes 4}$ ), since the seed theory is irrational and thus itself has an infinite number of boundary states. Furthermore, the boundary entropy of a typical state would (at the orbifold point) have a divergence proportional to  $N \log N$  as  $N \rightarrow \infty$  stemming from both the overall  $\frac{1}{\sqrt{N!}}$  normalization and the combinatorics. Thus, such boundary states would not describe an interface with a good geometric description.

From the discussion of [15], the boundary state encoding the Janus interface would be “atypical.” The coefficients of the twisted-sector terms would be given by characters of some representation of  $S_N$  because all  $N$  seed states are identical. For the large- $N$  boundary entropy at the orbifold point to be consistent with the gravitational calculation (4.1) (or more specifically, its order- $N$  scaling as  $N \rightarrow \infty$ ), the representation of  $S_N$  from which the coefficients are determined would need to have a dimension

$$d_{\text{rep}} \sim N^{N/2}, \quad N \rightarrow \infty, \quad (4.3)$$

thereby eliminating any imprint of the twisted-sector terms.

It would be interesting to understand more precisely the form of the boundary state describing the Janus interface. We do not anticipate transport coefficients being helpful towards this goal due to their expected sensitivity to coupling. However, we expect that calculations of boundary entropy for more stringy states (i.e. with a weak marginal coupling

turned on [57]) could probe more of the parameter space in Figure 3, thereby revealing more information about the twisted-sector coefficients in the boundary state. Along these lines, it would be interesting to consider the feasibility of applying the tensionless string program (particularly [16]) in a Janus background.

### 4.3 Other future directions

We also briefly describe some other directions for follow-up work.

**Twisted-sector data** The boundary entropy and transport coefficients involve overlaps of boundary states with untwisted states (respectively the vacuum and its level-2 spinless descendants). In symmetric orbifold theories, one could also examine the analogous twisted-sector overlaps. For example, we can define “twisted”  $g$ -functions as overlaps of the boundary state with a bare twist or “twisted” transport matrices in terms of overlaps of the boundary state with full Virasoro descendants of bare twists. It should also be possible to define “fractional” transport matrices in terms of fractional Virasoro generators.

**Other boundary data** One could study other types of data besides entropy or transport. For example, there is “defect complexity” [58]. This has been studied in the Janus solution through different prescriptions by [59, 60]. It would be interesting to see if similar quantities could be realized directly in the symmetric orbifold theory at the orbifold point.

**Entanglement in ICFT** Transport is only one example of physics made manifest by the presence of an interface. We can study other facets of ICFT, such as entanglement entropy [61, 62]. The question is then whether entanglement entropy generically encodes more information about the conformal interface beyond the boundary entropy of the associated boundary state.

### Acknowledgements

We thank Alexandre Belin, Shovon Biswas, Elena Cáceres, and Andreas Karch for useful discussions. We are also grateful to Constantin Bachas, Shira Chapman, and Andreas Karch for providing feedback on the draft. The work of SB was supported in part by the U.S. Department of Energy under Grant DE-SC0022021 and by a grant from the Simons Foundation (Grant 651440, AK). SS is supported by National Science Foundation (NSF) Grant No. PHY-2112725. SB and SS are also both supported by NSF Grant No. PHY-1914679.

## References

- [1] J. L. Cardy, *Conformal Invariance and Surface Critical Behavior*, *Nucl. Phys. B* **240** (1984) 514.
- [2] J. L. Cardy, *Boundary conformal field theory*, [hep-th/0411189](#).
- [3] I. Affleck, *Conformal field theory approach to the Kondo effect*, *Acta Phys. Polon. B* **26** (1995) 1869 [[cond-mat/9512099](#)].
- [4] I. Affleck, *Conformal field theory approach to quantum impurity problems*, in *Field Theories for Low-Dimensional Condensed Matter Systems: Spin Systems and Strongly Correlated Electrons*, (Berlin, Heidelberg), pp. 117–141, Springer Berlin Heidelberg, 2000, [DOI](#).
- [5] A. Sagnotti, *Open Strings and their Symmetry Groups*, in *NATO Advanced Summer Institute on Nonperturbative Quantum Field Theory (Cargese Summer Institute)*, (9, 1987), [hep-th/0208020](#).
- [6] J. Polchinski, *Dirichlet Branes and Ramond-Ramond charges*, *Phys. Rev. Lett.* **75** (1995) 4724 [[hep-th/9510017](#)].
- [7] M. R. Gaberdiel, *D-branes from conformal field theory*, *Fortsch. Phys.* **50** (2002) 783 [[hep-th/0201113](#)].
- [8] A. Recknagel and V. Schomerus, *Boundary Conformal Field Theory and the Worldsheet Approach to D-Branes*, Cambridge Monographs on Mathematical Physics. Cambridge University Press, 11, 2013, [10.1017/CBO9780511806476](#).
- [9] I. Affleck and A. W. W. Ludwig, *Universal noninteger ‘ground state degeneracy’ in critical quantum systems*, *Phys. Rev. Lett.* **67** (1991) 161.
- [10] E. Wong and I. Affleck, *Tunneling in quantum wires: A Boundary conformal field theory approach*, *Nucl. Phys. B* **417** (1994) 403 [[cond-mat/9311040](#)].
- [11] M. Oshikawa and I. Affleck, *Boundary conformal field theory approach to the critical two-dimensional Ising model with a defect line*, *Nucl. Phys. B* **495** (1997) 533 [[cond-mat/9612187](#)].
- [12] T. Azeyanagi, A. Karch, T. Takayanagi and E. G. Thompson, *Holographic calculation of boundary entropy*, *JHEP* **03** (2008) 054 [[0712.1850](#)].
- [13] T. Quella, I. Runkel and G. M. T. Watts, *Reflection and transmission for conformal defects*, *JHEP* **04** (2007) 095 [[hep-th/0611296](#)].
- [14] M. Meineri, J. Penedones and A. Rousset, *Colliders and conformal interfaces*, *JHEP* **02** (2020) 138 [[1904.10974](#)].
- [15] A. Belin, S. Biswas and J. Sully, *The spectrum of boundary states in symmetric orbifolds*, *JHEP* **01** (2022) 123 [[2110.05491](#)].
- [16] M. R. Gaberdiel, B. Knighton and J. Vošmera, *D-branes in  $AdS_3 \times S^3 \times \mathbb{T}^4$  at  $k = 1$  and their holographic duals*, *JHEP* **12** (2021) 149 [[2110.05509](#)].
- [17] F. M. Haehl and M. Rangamani, *Permutation orbifolds and holography*, *JHEP* **03** (2015) 163 [[1412.2759](#)].
- [18] A. Belin, C. A. Keller and A. Maloney, *String Universality for Permutation Orbifolds*, *Phys. Rev. D* **91** (2015) 106005 [[1412.7159](#)].

- [19] S. G. Avery, B. D. Chowdhury and S. D. Mathur, *Deforming the D1D5 CFT away from the orbifold point*, *JHEP* **06** (2010) 031 [[1002.3132](#)].
- [20] J. M. Maldacena, *The Large N limit of superconformal field theories and supergravity*, *Adv. Theor. Math. Phys.* **2** (1998) 231 [[hep-th/9711200](#)].
- [21] L. Eberhardt, M. R. Gaberdiel and R. Gopakumar, *Deriving the  $AdS_3/CFT_2$  correspondence*, *JHEP* **02** (2020) 136 [[1911.00378](#)].
- [22] M. Chiodaroli, M. Gutperle and D. Krym, *Half-BPS Solutions locally asymptotic to  $AdS(3) \times S^{*3}$  and interface conformal field theories*, *JHEP* **02** (2010) 066 [[0910.0466](#)].
- [23] M. Chiodaroli, M. Gutperle and L.-Y. Hung, *Boundary entropy of supersymmetric Janus solutions*, *JHEP* **09** (2010) 082 [[1005.4433](#)].
- [24] D. Bak, M. Gutperle and S. Hirano, *Three dimensional Janus and time-dependent black holes*, *JHEP* **02** (2007) 068 [[hep-th/0701108](#)].
- [25] C. Bachas, S. Chapman, D. Ge and G. Policastro, *Energy Reflection and Transmission at 2D Holographic Interfaces*, *Phys. Rev. Lett.* **125** (2020) 231602 [[2006.11333](#)].
- [26] S. A. Baig and A. Karch, *Double brane holographic model dual to 2d ICFTs*, *JHEP* **10** (2022) 022 [[2206.01752](#)].
- [27] C. Bachas, S. Baiguera, S. Chapman, G. Policastro and T. Schwartzman, *Energy transport for thick holographic branes*, [2212.14058](#).
- [28] S. S. Gubser, I. R. Klebanov and A. A. Tseytlin, *Coupling constant dependence in the thermodynamics of  $N=4$  supersymmetric Yang-Mills theory*, *Nucl. Phys. B* **534** (1998) 202 [[hep-th/9805156](#)].
- [29] A. Fotopoulos and T. R. Taylor, *Comment on two loop free energy in  $N=4$  supersymmetric Yang-Mills theory at finite temperature*, *Phys. Rev. D* **59** (1999) 061701 [[hep-th/9811224](#)].
- [30] G. Policastro, D. T. Son and A. O. Starinets, *The Shear viscosity of strongly coupled  $N=4$  supersymmetric Yang-Mills plasma*, *Phys. Rev. Lett.* **87** (2001) 081601 [[hep-th/0104066](#)].
- [31] A. Buchel, J. T. Liu and A. O. Starinets, *Coupling constant dependence of the shear viscosity in  $N=4$  supersymmetric Yang-Mills theory*, *Nucl. Phys. B* **707** (2005) 56 [[hep-th/0406264](#)].
- [32] S. C. Huot, S. Jeon and G. D. Moore, *Shear viscosity in weakly coupled  $N = 4$  super Yang-Mills theory compared to QCD*, *Phys. Rev. Lett.* **98** (2007) 172303 [[hep-ph/0608062](#)].
- [33] B. A. Burrington, I. T. Jardine and A. W. Peet, *The OPE of bare twist operators in bosonic  $S_N$  orbifold CFTs at large  $N$* , *JHEP* **08** (2018) 202 [[1804.01562](#)].
- [34] B. A. Burrington and A. W. Peet, *Fractional Conformal Descendants and Correlators in General 2D  $S_N$  Orbifold CFTs at Large  $N$* , [2211.04633](#).
- [35] A. Recknagel, *Permutation branes*, *JHEP* **04** (2003) 041 [[hep-th/0208119](#)].
- [36] N. Ishibashi, *The Boundary and Crosscap States in Conformal Field Theories*, *Mod. Phys. Lett. A* **4** (1989) 251.
- [37] T. Onogi and N. Ishibashi, *Conformal Field Theories on Surfaces With Boundaries and Crosscaps*, *Mod. Phys. Lett. A* **4** (1989) 161.
- [38] C. Bachas, Z. Chen and V. Papadopoulos, *Steady states of holographic interfaces*, *JHEP* **11** (2021) 095 [[2107.00965](#)].

- [39] T. Anous, M. Meineri, P. Pelliconi and J. Sonner, *Sailing past the End of the World and discovering the Island*, *SciPost Phys.* **13** (2022) 075 [[2202.11718](#)].
- [40] G. T. Horowitz, J. M. Maldacena and A. Strominger, *Nonextremal black hole microstates and  $U$  duality*, *Phys. Lett. B* **383** (1996) 151 [[hep-th/9603109](#)].
- [41] N. Seiberg and E. Witten, *The  $D1 / D5$  system and singular CFT*, *JHEP* **04** (1999) 017 [[hep-th/9903224](#)].
- [42] J. R. David, G. Mandal and S. R. Wadia, *Microscopic formulation of black holes in string theory*, *Phys. Rept.* **369** (2002) 549 [[hep-th/0203048](#)].
- [43] K. Skenderis and S. N. Solodukhin, *Quantum effective action from the AdS / CFT correspondence*, *Phys. Lett. B* **472** (2000) 316 [[hep-th/9910023](#)].
- [44] K. Skenderis, *Asymptotically Anti-de Sitter space-times and their stress energy tensor*, *Int. J. Mod. Phys. A* **16** (2001) 740 [[hep-th/0010138](#)].
- [45] I. Papadimitriou and K. Skenderis, *Correlation functions in holographic RG flows*, *JHEP* **10** (2004) 075 [[hep-th/0407071](#)].
- [46] J. Estes, K. Jensen, A. O’Bannon, E. Tsatis and T. Wrase, *On Holographic Defect Entropy*, *JHEP* **05** (2014) 084 [[1403.6475](#)].
- [47] M. Gutperle and A. Trivella, *Note on entanglement entropy and regularization in holographic interface theories*, *Phys. Rev. D* **95** (2017) 066009 [[1611.07595](#)].
- [48] L. Randall and R. Sundrum, *An Alternative to compactification*, *Phys. Rev. Lett.* **83** (1999) 4690 [[hep-th/9906064](#)].
- [49] A. Karch and L. Randall, *Locally localized gravity*, *JHEP* **05** (2001) 008 [[hep-th/0011156](#)].
- [50] C. Bachas, J. de Boer, R. Dijkgraaf and H. Ooguri, *Permeable conformal walls and holography*, *JHEP* **06** (2002) 027 [[hep-th/0111210](#)].
- [51] D. Bak, M. Gutperle and S. Hirano, *A Dilatonic deformation of AdS(5) and its field theory dual*, *JHEP* **05** (2003) 072 [[hep-th/0304129](#)].
- [52] A. Clark and A. Karch, *Super Janus*, *JHEP* **10** (2005) 094 [[hep-th/0506265](#)].
- [53] S. Ryu and T. Takayanagi, *Holographic derivation of entanglement entropy from AdS/CFT*, *Phys. Rev. Lett.* **96** (2006) 181602 [[hep-th/0603001](#)].
- [54] A. Belin, N. Benjamin, A. Castro, S. M. Harrison and C. A. Keller,  *$\mathcal{N} = 2$  Minimal Models: A Holographic Needle in a Symmetric Orbifold Haystack*, *SciPost Phys.* **8** (2020) 084 [[2002.07819](#)].
- [55] N. Benjamin, S. Bintanja, A. Castro and J. Hollander, *The stranger things of symmetric product orbifold CFTs*, *JHEP* **11** (2022) 054 [[2208.11141](#)].
- [56] A. Belin, A. Castro, C. A. Keller and B. Mühlmann, *The Holographic Landscape of Symmetric Product Orbifolds*, *JHEP* **01** (2020) 111 [[1910.05342](#)].
- [57] M. R. Gaberdiel, C. Peng and I. G. Zadeh, *Higgsing the stringy higher spin symmetry*, *JHEP* **10** (2015) 101 [[1506.02045](#)].
- [58] S. Chapman, D. Ge and G. Policastro, *Holographic Complexity for Defects Distinguishes Action from Volume*, *JHEP* **05** (2019) 049 [[1811.12549](#)].
- [59] R. Auzzi, S. Baiguera, S. Bonansea, G. Nardelli and K. Toccacelo, *Volume complexity for Janus  $AdS_3$  geometries*, *JHEP* **08** (2021) 045 [[2105.08729](#)].

- [60] R. Auzzi, S. Baiguera, S. Bonansea and G. Nardelli, *Action complexity in the presence of defects and boundaries*, *JHEP* **02** (2022) 118 [[2112.03290](#)].
- [61] A. Karch, Z.-X. Luo and H.-Y. Sun, *Universal relations for holographic interfaces*, *JHEP* **09** (2021) 172 [[2107.02165](#)].
- [62] A. Karch and M. Wang, *Universal Behavior of Entanglement Entropies in Interface CFTs from General Holographic Spacetimes*, [2211.09148](#).